Effects of Spin and Mass Addition on High-Angle-of-Attack Re-entry

A.M. Morrison* and C. Fiscina†
Naval Surface Weapons Center, White Oak, Silver Spring, Maryland

A series of wind tunnel experiments has been conducted to investigate boundary layer and mass addition effects on the aerodynamics of typical re-entry configurations. Early investigators hypothesized that skewed circumferential mass addition distributions which might result from hypersonic ablation, at angle of attack, with spin could result in a Magnus-like side force and moment. The experiments described here were conducted in the Naval Surface Weapons Center Hypervelocity Research Tunnel at a Mach number of 18. Results of experiments in which both qualitative and quantitative simulations were carried out will be presented in the form of aerodynamic forces and moments in the pitch and yaw planes. This unique data base is a valuable tool in ongoing flowfield modeling/validation efforts.

Nomenclature

A	= model reference area, in.^{2}
d	= base diameter, in.
KN	= Knudsen number $\{M/\sqrt{(Re/\text{ft}) \times (\text{LREF})}\}$
LREF	= model reference length, in.
M	= Mach number
MRC	= moment reference center, in.
$\dot{m}$	= total blowing rate, lbm/ft^2-s
P_o	= supply pressure, psia
Q	= freestream dynamic pressure, psia
Re/ft	= Reynolds number per foot
r_B	= model base radius in.
r_n	= model nose radius, in.
S	= distance along model surface from stag. pt., in.
T	= supply temperature, °R
V	= freestream velocity, ft/s
XCP, XCPP	= distance from nosetip of model to normal force center of pressure divided by LREF
YCP	= distance from nosetip of model to side force center of pressure divided by LREF
α	= angle of attack, deg
α_E	= angle of attack at entry, deg
ϕ	= angle of peak in blowing distribution from windward ray
τ	= pitching and yawing frequency
ρ	= freestream density

Introduction

UNDERSTANDING, modeling, and predicting the accuracy of high-performance reentry systems have been the goals of a number of recent programs throughout the strategic community. One area which has been identified as a result of such studies is the ability to predict with confidence the high angle of attack performance of vehicles re-entering the Earth's atmosphere in the altitude regime between 400,000 and 100,000 ft. The earliest investigators applied the method of Newton[1] in order to predict the aerodynamics of meteorites and man-made vehicles as they passed through the high-altitude regime. The requirement for increased accuracy in predicting high-altitude performance led to the development of more complex technique.[2-4] Investigators also noticed anomalous aerodynamic effects in ground and flight experiments[5,6] The referenced flight test experience involved two tests of the English Black Knight Re-entry Vehicle. These were the RV's of BK09 and BK18. Both vehicles were 12½ deg half-angle blunted cones, with 15.4-in.-diam bases and 2-in. radius nose and nominal hypersonic static margins of 1.5 in. The heat shield was composed of phenolic resin reinforced with asbestos flock. RV-BK09 was also painted with Araldite to prevent outgassing affecting a sensitive pressure gage used to initiate its reentry boost motor. RV-BK09, flown in 1960, re-entered at a speed of 15,000 ft/s, experienced a dynamic instability at 140,000 ft which grew until the vehicle became dynamically unstable and subsequently broke up at 70,000 ft. The re-entry vehicle also experienced windward meridian temperatures that would cause the Araldite paint to char and inject mass in to the vehicle boundary layer at an altitude of 140,000 ft. The RV-BK18 was flown to check some of the problems raised by RV-BK09. It carried extensive instrumentation and excellent quality data were obtained. The BK18 was not painted with Araldite. No dynamic effects were exhibited in the region where BK09 experienced dynamic instabilities. At about 85,000 ft, vehicle dynamics cause a divergence in the angle of attack. The altitude where ablation of the phenolic afterbody heatshield was expected is at 85,000 ft. Six-degree-of-freedom trajectory simulation of BK18 and BK09 were attempted postflight. Agreement with flight-observed performance could be obtained in the regions of observed dynamic instability only when a Magnus-like term was included in the equations of motion. The size of the required Magnus term was much too large to be physically explained as a classical Magnus phenomenon. It was, therefore, proposed that the source of the Magnus-like term was an out-of-plane pitching moment associated with the charing or ablation of the Araldite phenolic heatshield. A new ablation pitching moment derivative, $C_{ma\dot{\alpha}}$, and as associated time lag, τ, were proposed.

Prior to this investigation, mass addition-induced lagging moments were generally believed to affect only the dynamic stability derivative C_{mq}. The C_{mq} effect has been demonstrated in ground tests.[5]

The purpose of the present paper is to investigate dynamic ablation effects on modern re-entry configuration in a series of ground experiments. The first experiment provides a proof-of-principle demonstration for the phenomena described

Presented as Paper 82-0190 at the AIAA 20th Aerospace Sciences Meeting, Orlando, Fla., Jan. 11-14, 1982; received Jan. 22, 1982; revision received Mach 22, 1984. This paper is declared a work of the U.S. Government and therefore is in the public domain.

*Head, Re-entry Systems Branch. Associate Fellow AIAA.
†Aerodynamic Facilities Group Leader. Member AIAA.

above. The next series of experiments provide quantitative data for model formulation and flowfield code validation. Finally, results from the ground experiments are used in six-degree-of-freedom trajectory simulations to assess re-entry system performance implications.

Ablation Lag Moments

The injection of mass into the boundary layer of a re-entry vehicle traveling at high speed can influence aerodynamic forces by altering both the skin friction and induced pressure effects of boundary layer displacement. The combined effets of mass addition, spin, and angle of attack can produce a mechanism which can lead to out-of-plane forces and moments as illustrated in Fig. 1. The windward side of the re-entry vehicle would first experience the temperature and pressure necessary to induce mass addition. Once the re-entry vehicle heat shield experienced these conditions, a finite period of time would be required for the material to respond and eject mass. In the case of a spinning re-entry vehicle, this material lag would cause the rate of mass addition to be higher on one side of the vehicle than the other, in that as an outgassing ray moves to the lee ray, the temperature and pressure decrease, as do the rate and magitude of mass addition. The differential mass addition rate and magnitude cause the side of the higher mass addition to have a thicker boundary layer. The boundary layer asymmetry leads to an induced pressure force and moment. The resultant force acts in a direction opposite to that of a classical Magnus force.

In general, the aerodynamic shear associated with a thin boundary layer is larger than that associated with a thicker boundary layer. A shear couple, therefore, also results due to the longitudinal shear differential associated with the high and low mass addition sides of the vehicle. Radial shear differential would also create a couple opposing roll.

Proof-of-Principle Experiment

Ablating and nonablating spherically blunted cone models were tested at Mach 18 in the Naval Surface Weapons Center Hypervelocity Research Tunnel.[7] Details of the configuration tested are shown in Fig. 2. Camphor was used as an ablating material. Thin steel model shells were fabricated with a 0.32-cm layer of camphor covering 86.9% of the body length, as shown in Fig. 2. Aluminum shell was fabricated for the nonablating model. A steel nose tip was for the ablating models as well as for the nonablating model to avoid shape change effects in the region of highest aerodynamic heating. The static force measurements were made with a four-component strain gage force balance which was designed for the test program and incorporated a mechanism for spinning the models.

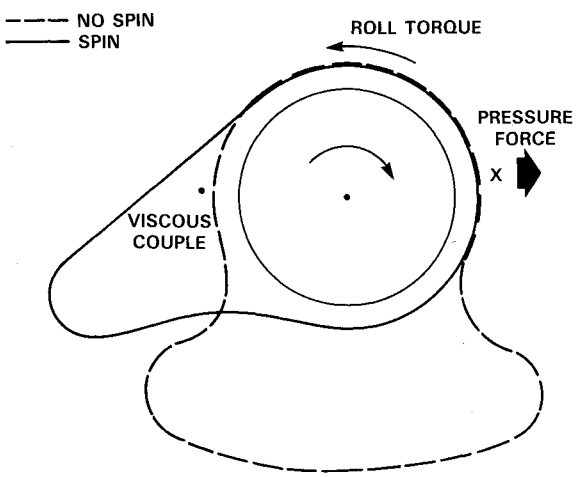

Fig. 1 Side force and moment development.

The test procedure consisted of spinning the model to the desired rate while bringing the wind tunnel supply pressure and temperature to the run condition. During this startup period the model was kept in a retracted position in the test cell of the open-jet wind tunnel. When the run conditions were achieved, the model was injected into the tunnel flow, and force data were recorded while the angle of attach was swept at a rate of roughly 1.5 deg/s up to a maximum value which depended on the tunnel supply pressure. During the most of the ablating model tests the sweep was halted for a few seconds at 10 and 25 deg angle of attack in order to look for possible transient effects. After completing the data sweep it was necessary to return the model to a small angle of attack before retracting it from the tunnel flow. As a result, the amount of camphor ablated during the data sweep could not be determined. Usually all the camphor was ablated during the wind tunnel run and shutdown process. Observation via a television monitor indicated that the camphor-coated portion of the models remained fully coated throughout the data sweep. Models examined after two aborted runs indicated that roughly 20-30% of the camphor could have ablated prior to the data sweep as a result of exposure to the low-pressure test cell environment.

The side force data obtained from the wind tunnel experiments are given in Fig. 3 as plots of yaw force coefficient YFC vs angle of attack. Data taken during the pauses in the angle of attack sweeps at 10 and 25 deg agreed very well with the data taken during the continuous pitch sweeps, thereby verifying the sweeping technique. Comparisons made among data from ablating and nonablating model experiments clearly indicated a significant side force due to ablation. The ablating model data also indicated that the side force is a strong function of the angle of attack—nonlinear up to about 10 deg and linear at higher angles. Data were gathered at spin rates between 1 and 7 rps. For camphor ablation at the test conditions reported here, the side force due to ablation was

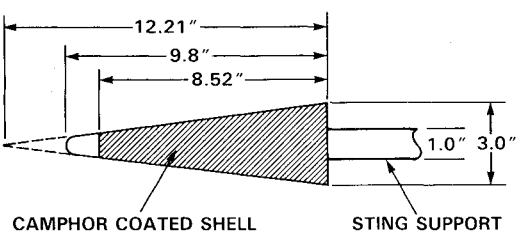

Fig. 2 Mach 18 camphor model.

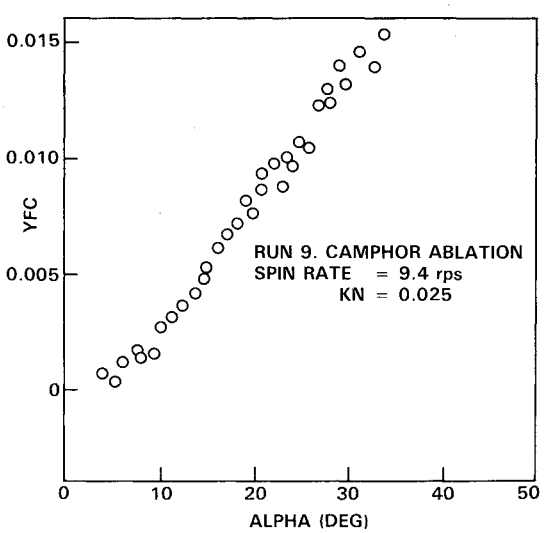

Fig. 3 Proof-of-principle experimental results.

independent of spin rate at speeds greater than 1-2 rps for angles of attack up to 25 deg.

The data show the angle of attack behavior of the side force due to ablation to be very similar to that of the normal force, and the magnitude of the side force to be roughly 1% of the normal force. The response of the camphor ablation to changes in angle of attack was evidently quite rapid since the data taken at fixed angle of attack do not indicate any large lag effects.

In the wind tunnel, positive angle of attack was nose-up. The direction of spin was clockwise, looking upstream. The direction of the observed side force was to the right, looking upstream, which is in agreement with the qualitative mechanism for the ablation-induced side force previously mentioned.

The center of pressure of the side force was also measured, but due to the fact that the force was very small, accurate results were not obtained. In general, the experimental data indicate the side force center of pressure to be located 50-60% of the body length from the nose tip and independent of the angle of attack.

Normal force and pitch center of pressure measurements were also made, and the results for the ablating models were in good agreement with those for the nonablating models. The normal force data were in good agreement with classical Newtonian flow theory. The center of pressure data for the ablating models showed small shifts ($< \frac{1}{2}\%$ of body length), while the angle of attack was held constant at 10 and 25 deg. These shifts are believed to be due to the effect of shape change.

The shape change effects and the inability to characterize the mass addition parameters of the camphor during the experiment classify the camphor results as qualitative. They do, however, provide a proof-of-principle demonstration of the lag moment effect.

Quantitative Experiments

Porous Model Design

The model used in this experiment was a hemispherically blunt cone with a half-angle of 7 deg and a bluntness ratio, r_n/r_B, of 0.223. Figure 4 shows a schematic of the model. It incorporates a solid stainless steel nose cap and a porous stainless steel outer shell, through which nitrogen is forced in a prescribed circumferential and axial distribution and flow rate simulating heatshield mass addition. The model is mounted on a specially built four-component internal strain gage balance for measurement of the aerodynamic force and moments in both the pitch and yaw planes. Its instrument components are solid state strain gages, which have a much higher output than the conventional foil gages. This higher output was necessary since the side force were anticipated to be less than 0.1 lb. The balance has two 0.2-in. internal diameter tubes through the center which permit gas to be fed through the balance with no effect on balance output. This gas is fed to the flow distributor section, shown in Fig. 5, which distributes the gas to the eight chambers of the inner shell at differenct rates through sonic orifices of different diameters. The gas then flows through the porous outer shell in a manner similar to outgassing from an actual re-entry vehicle heat-shield.

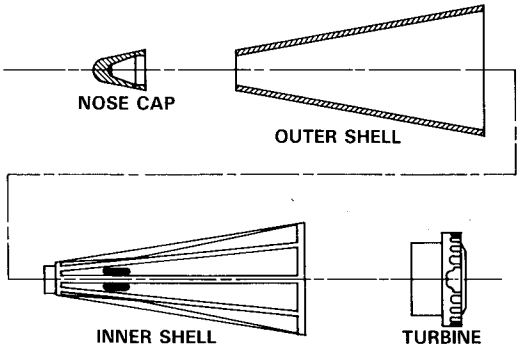

Fig. 4 Schematic of porous model.

Blowing Distribution

Prior to running the test, measurements were made of the outgassing distribution obtained at four axial stations on the model. To measure the rate of outgassing, a sampling tube of a known diameter was pressed against the porous shell. This tube was connected to a calibrated orifice with a diameter of 0.020 in. The entire model and calibration system were placed in a vaccum chamber at a static pressure of 8 mm Hg. The pressure upstream of the calibrated orifice was measured and

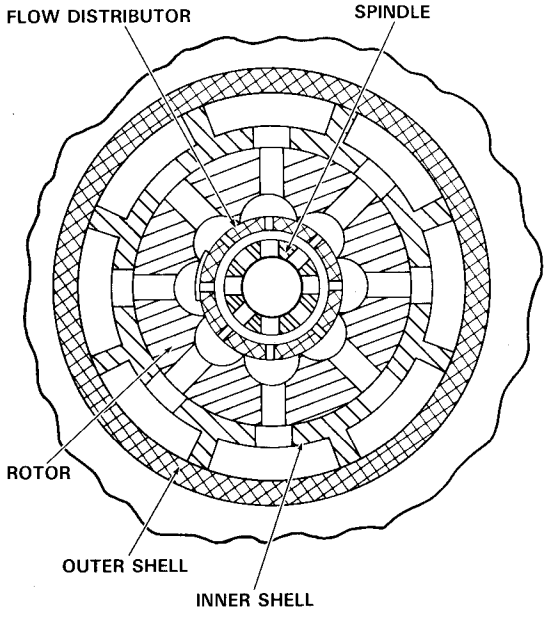

Fig. 5 Flow distributor.

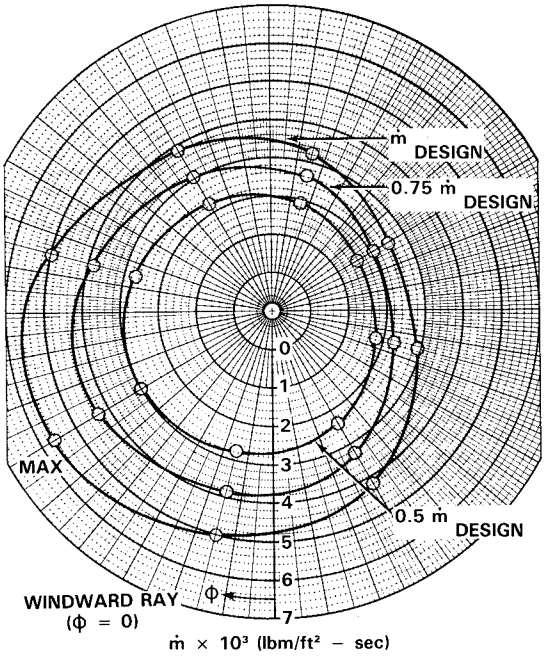

Fig. 6 Measured blowing distribution at forward station, $S/RN = 8.25$.

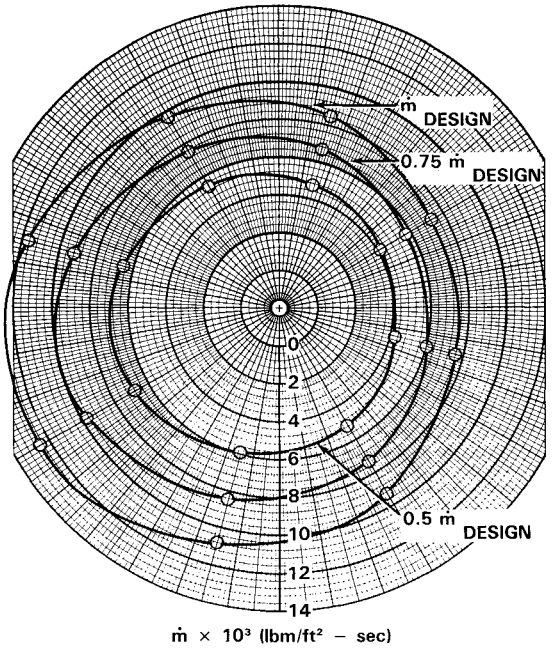

Fig. 7 Measured blowing distribution at aft station, $S/RN=27$.

used to calculate the mass flow, $\dot{m}$, from the relation

$$\dot{m}\frac{\text{lbm}}{\text{s}} = \frac{0.532P(\text{psi})A_*(\text{in.})}{\sqrt{T_o\,(^\circ\text{R})}}$$

Figures 6 and 7 show the measured distribution at two of the axial stations. The distribution has a maximum at 60 deg from the windward ray with a minimum at 240 deg. The orientation of the distribution can be changed by rotating the internal flow distributor described in the previous section. Three blowing rates are shown, indicating the rates at which tests were conducted.

Test Conditions

This test was conducted in the Naval Surface Weapons Center Hypervelocity Research Tunnel at a Mach number of 18. The supply conditions were $P_o=450$ atm and $T_o=3000^\circ$F, producing a freestream Reynolds number per foot of 0.5×10^6 and a Knudsen number of 0.025. Static force and moment measurements were made at six angles of attack from 0 through 25 deg and two orientations of the blowing distribution. The tunnel conditions and model data are shown in Tables 1 and 2.

Results and Discussion

The static force data for a typical run are presented in Table 3. Upon examination of the tabulated data it is evident that the calculated yaw plane forces and moments begin to drift after approximately one second of exposure time to the tunnel flow at high angle of attack. It has been determined that this was caused by the output of the force balance changing due to a change in temperature. This change in temperature was due to impingement of the strong bow shock on the sting just behind the model. This effect was accounted for by using only the first second of data before the drift began. Later wrapping the sting with insulation virtually eliminated this problem.

Figures 8 and 9 show the normal force and center of pressure coefficients plotted against angle of attack. Analytical values obtained from classical Newtonian theory (CPMAX = 2) and from an inviscid flow field computer code are also presented. Excellent agreement is observed in all cases between the data and the predictions.

Table 1 Tunnel conditions

Supply pressure, atm	450
Supply temperature, °F	3000
Dynamic pressure, psi	0.615
Freestream velocity, ft/s	7200
Re/ft	0.52×10^6
Knudsen number	0.025

Table 2 Model data

Cone half-angle, deg	7.0
Bluntness ratio	0.223
Base diameter, in.	3.0
Length, in.	9.8
Porous section, length, in.	8.0
Nose radius, in.	0.335
Moment reference point, in. from nose	5.831

Table 3 Tabulated data from typical run[a]

Time, s	Normal force coefficient, NFC	Pitching moment coefficient, PMC	Yaw force coefficient, YFC	Yaw moment coefficient, YMC
0.0	1.0021	−0.0666	−0.0038	−0.0011
0.2	1.0018	−0.0666	−0.0040	−0.0010
0.4	1.0034	−0.0666	−0.0041	−0.0012
0.6	1.0026	−0.0658	−0.0043	−0.0012
0.8	1.0041	−0.0661	−0.0042	−0.0013
1.0	1.0042	−0.0655	−0.0045	−0.0013
2.0	1.0037	−0.0652	−0.0050	−0.0015
3.0	1.0059	−0.0643	−0.0064	−0.0017
4.0	1.0058	−0.0639	−0.0088	−0.0018
5.0	1.0090	−0.0649	−0.0111	−0.0018

[a] $\alpha=25$ deg; $\phi=60$ deg

The side forces and moments plotted against angle-of-attack are shown in Fig. 10 and 11. When the blowing was oriented with the peak at 60 deg from the windward ray, a side force coefficient was measured at approximately 0.005 over the entire range of angles of attack tested. This contrasts the earlier camphor model test where the side forces increased with increasing angle of attack. This difference was due to the skewed blowing distribution being generated internally in the later test so that it existed even in a zero angle of attack. With the camphor model, the skewed distribution exists only when the model experiences asymmetric heating at angle of attack and while spinning.

Changing the orientation of blowing distribution by moving the peak closer to the windward ray reduces the magnitude of the side forces measured. This indicates that a change in the thermal lag properties of a heatshield material would alter the aerodynamics of the re-entry vehicle.

Figure 12 shows the sides forces data at an angle of attack of 25 deg for the three different mass addition rates tested. Here again, we see a change in the force due to a change in the mass addition characteristics, indicating that the heatshield material plays a major role in determining the high-altitude performance of a re-entry vehicle.

Remaining Technology Issues

Some of the issues which remain to be addressed include the effects of simultaneous spin and mass addition, axial variations of the mass addition distribution, and leeside flowfield physics as well as flowfield modeling on the leeward side of a vehicle at angle of attack.

The issue of axial variation of the mass addition distribuiton is being addressed in an ongoing test. The axial

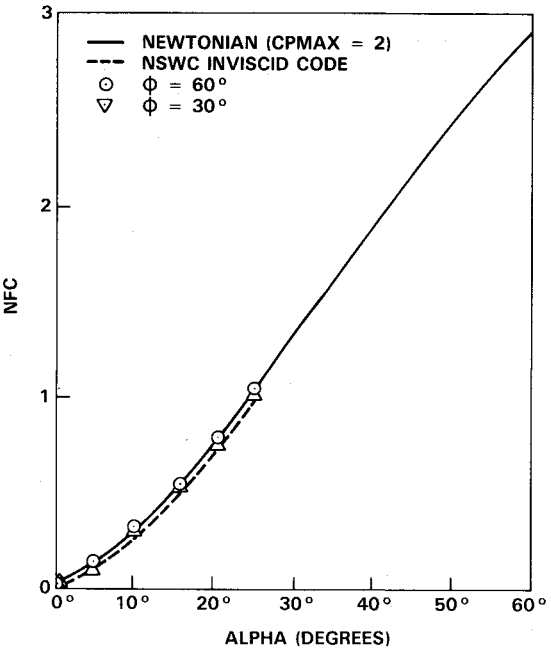

Fig. 8 Normal force coefficient vs alpha.

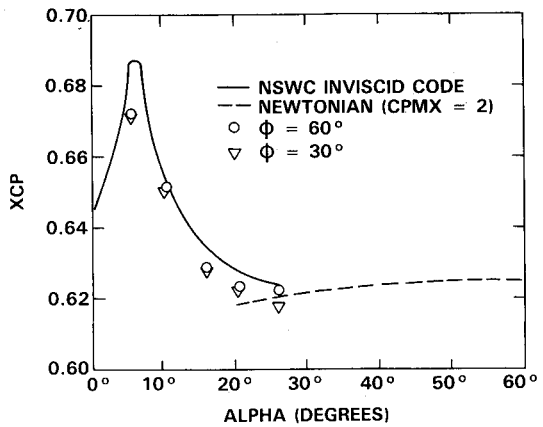

Fig. 9 Center of pressure coefficient vs alpha.

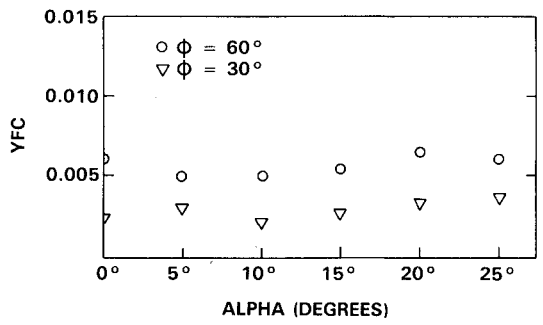

Fig. 10 Side force coefficient vs alpha.

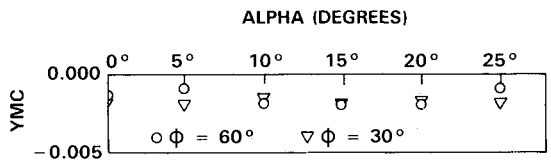

Fig. 11 Side moment coefficent vs alpha.

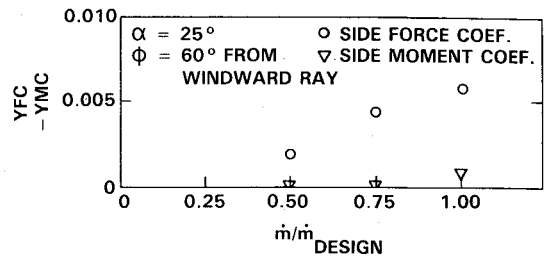

Fig. 12 Side force and moment coefficient for various blowing rates.

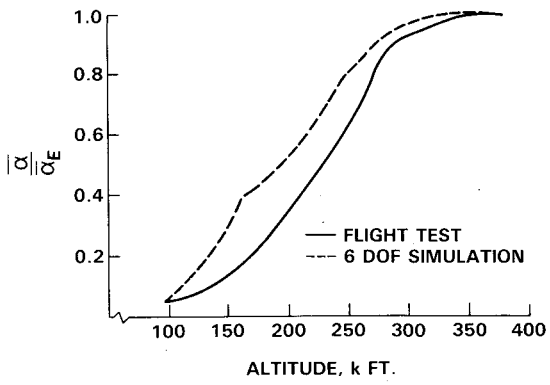

Fig. 13 Alpha vs altitude.

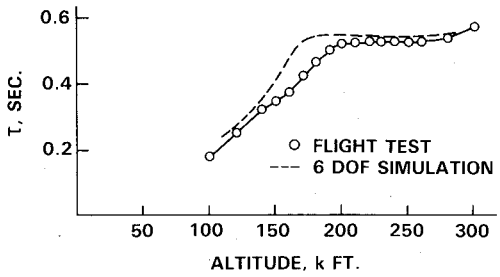

Fig. 14 Frequency vs altitude.

distribution in the previous test was such that the magnitude of mass addition became larger at the rear of the model than at the nose. This is contrary to the distribution over an actual re-entry vehicle; hence, an new model is under development which will model the axial mass addition distribution correctly.

Trajectory Simulations

Results from the quantitative wind tunnel experiments were input to a six-degree-of-freedom trajectory simulator in the form of out-ot-plane forces and moments as suggested in Ref. 6. Catastrophic dynamic instabilities as observed in the Black Knight flight test were not obtained for modern re-entry vehicle stability and blowing parameters. The effect of the out-of-plane moment was to cause the precessional oscillation of the re-entry vehicle to damp faster that the nominal simulation without the side moment modeled. The vehicle pitching and yawing frequency was also altered. These results are shown in Figs. 13 and 14. The faster damping reduced re-entry system drag due to angle of attack. This resulted in the re-entry vehicle with the side moment overflying the impact point of the re-entry vehicle without the side moment. A parametric study was also conducted in order to determine if the performance with the side moment could be simulated by varyng C_{mq}, X_{cp}, and normal force. As in Ref. 6, the side moment generated performance could not be simulated.

Summary

Ablation lag moments as observed in the Black Knight Re-entry Vehicle flight test program have been investigated. A force and moment system has been proposed to account for the ablation lag aerodynamics. A proof-of-principle wind tunnel experiment has been conducted to demonstrate the existence of the ablation lag force and moments. A quantitative data base has been generated for modern re-entry system aerodynamic and blowing parameters. Results from the experiments were used to gain insight into the effects of ablation lag moments on re-entry system performance. The effects of the out-of-plane moment were increased damping and altered pitching and yawing frequencies.

Acknowledgments

This work was conducted under the Re-entry Technology Program Office of the Strategic Systems Department of the Naval Surface Weapons Center, Dr. W. Carson Lyons, Manager. The authors wish to acknowledge the contributions of J. Marshall, R. Voisinet, and Mary Ellen Falusi in the collection, processing, and reduction of the data contained in this report.

References

[1] Zahm, A. F., "Superaerodynamics," *Journal of the Franklin Institute,* Vol. 217, Jan. 1934, pp. 153-166.

[2] Tsien, H. S., "Superaerodynamics, Mechanics of Rarefied Gases," *Journal of the Aeronautical Sciences,* Vol. 13, Dec. 1946, pp. 653-664.

[3] Adams, M. C., and Probstein, R. F., "On the Validity of Continuum Theory for Satelite and Hypersonic Flight Problems at High Altitudes," *Jet Propulsion,* Vol. 6, Feb. 1958, pp. 86-89.

[4] Tan, H. S., "Nose Drag in Free-Molecular Flow and Its Minimization," *Journal of the Aerospace Sciences,* Vol. 26, June 1959, pp. 360-365.

[5] Ericsson, L. E., "Effect of Nose Bluntness on the Hypersonic Unsteady Aerodynamics of an Ablating Reentry Body," *Journal of Spacecraft and Rockets,* Vol. 4, June 1967, pp. 811-813.

[6] Waterfall, A. P., "Effect of Ablation on the Dynamics of Spinning Reentry Vehicles," *Journal of Spacecraft and Rockets,* Vol. 6, Sept. 1969, pp. 1038-1044.

[7] Ragsdale, W. C., and Horanoff, E. V., "Investigation of a Side Force Due to Ablation," *Journal of Spacecraft and Rockets,* Vol. 16, Sept. 1978, pp. 1010-1011.